博士論文(要約)

# Studies on a Functional-Structural Model for Determination of P-uptake and Utilization in Upland Rice
# (陸稲におけるリンの取り込みおよび利用効率を定量化するための機能構造モデルに関する研究)

ゴンザレス ロザーノ ギエルモ ダニエル

# Table of Contents:

# Chapter I: Introduction and Research Objectives

### 1.1 Rice in Africa

Rice consumption in Africa is increasing rapidly, leading to a widening gap between demand and local rice production (Nigatu et al. 2017). One reason for this widening gap is the relatively low rice productivity in Sub-Saharan Africa (SSA), which is due to a combination of low production inputs and unfavorable production environments (Saito et al. 2019). About 30% of the rice cropping area in Africa is in the more stress-prone uplands (Diagne et al. 2013) where irrigation is nor provided. The average upland rice yields in Africa are around 1.2 t $ha^{-1}$ (Drame et al. 2013) compared to an average of 4.75 t $ha^{-1}$ in irrigated rice in Asia in 2016.(IRRI World Rice Statistics, 2020).

African farmers producing upland rice are generally low-income farmers that acquire very limited amounts of fertilizers and other inputs (Tsujimoto at al. 2019). Their economic conditions exacerbate problems inherent to the uplands, where highly weathered soils such as Oxisols tend to bind phosphate (P) in plant-unavailable forms. High P fixation in soils coupled with low P fertilization rates cause P to be the primary limiting factor in the production of rice in SSA (Saito et al. 2019). It is therefore of utmost importance that rice varieties with improved P acquisition and utilization efficiency are developed, as these provide a cost-efficient partial solution to the soil fertility problem in SSA (VanDamme, 2015).

### 1. 2 P-Efficient Rice Characteristics

Screening experiments have shown that genotypic differences exist for tolerance to P deficiency in the rice germplasm (Fageria et al 2013, VanDamme et al. 2015) and that this can be caused by differences in P acquisition efficiency (Mori et al 2016), P utilization efficiency (Wissuwa et al. 2015) or by a combination of both (Rose et al. 2013). P acquisition was found to mainly depend on differences in root system size with smaller effects contributed by differences in P uptake efficiency characterized by superior P uptake per unit root size (Mori et al 2016; Wissuwa et al. 2020). One of the P deficiency tolerant rice genotypes combining vigorous seedling root growth with high P uptake efficiency is the gene bank accession ‘DJ123’ (Wissuwa et al. 2020). It originates from Bangladesh and belongs to the *aus* sub-species of rice that is well known as a source of donors for abiotic stress tolerance.

The size of a root system is the sum of its different components and in rice four main classes of roots are distinguished; main root axes are formed by the primary root and subsequent nodal roots (also called crown roots) and both classes give rise to two classes of lateral roots (Rebouillat et al. 2009). The larger L-type lateral roots contain several layers of cortex cells and typically have secondary or even tertiary branches while the small S-type lateral roots contain only one layer of cortical cells, are unbranched and short with a maximum of around 1 cm and a diameter smaller than 50 µm (Wissuwa et al. 2020). S-type laterals develop on both main axes and L-type laterals. They have so far only been reported for rice but not for other cereals. An order of magnitude finer than these S-type laterals are root hairs and recently Nestler et al. (2016) showed that these hairs develop on all root classes in rice, including on S-type roots, where they are present in high density but at slightly reduced length compared to hairs on the main axes. Experiments have shown that root hairs are directly involved in P uptake from the soil (Gahoonia and Nielsen, 1998) and that they are particularly effective in overcoming the combined effects of water and P deficiency stress (Brown et al., 2012). Considering that S-type lateral roots appear to be unique to rice, that these roots can

contribute more than half of the total root system length (Nestler et al. 2016), and that they are covered by even finer root hairs, it becomes evident that rice has a particularly high proportion and amount of very fine root structures exploring the soil for resources like water and nutrients, which should be especially beneficial for poorly mobile nutrients like P.

What is not known is to what extent each root class and the hairs developing on them contribute to total plant P uptake. It would be of interest from a plant breeding point to estimate to what extent changes in properties of different root classes and hairs would improve P uptake, as this would allow for the formulation of clear breeding targets with relation to which specific root system trait would provide the largest improvements in P uptake. For example, using a modeling approach Zygalakis et al. (2011) predicted that increasing root hair length would improve P uptake more than increasing root hair density. Genotypic differences in root hair length have been reported for rice grown in soil and gene bank accession DJ123 was found to have slightly longer hairs compared to other genotypes (Nestler & Wissuwa, 2016). To what extent genotypes differ in S-type lateral root development has not been investigated in detail.

**1.3 Computational Models**

While mathematical models and computational simulations of rice and rice growth have been ongoing for almost 30 years (Morita, 1994), to our knowledge, modeling studies have not yet addressed the effect of differences in S-type length and density in the presence of root hairs.

Recently, De Bauw et al. (2020) presented a functional-structural model that computes water and P uptake from an upland rice variety, Nerica4, utilizing CRootBox. They concluded that S-type laterals would indeed contribute prominently to P uptake. Furthermore, their main conclusion was that the total number of root tips growing into previously undepleted soil are the main contributors to overall P uptake from a low-P soil and that L-type laterals and the secondary branching from these L-type laterals may contribute significantly to total root tip number. The model developed by De Bauw et al. (2020) successfully predicted water and P uptake in a P-fertilized soil, but underestimated P uptake from an unfertilized low-P soil. They hypothesized that this underestimation may be due to four factors; not accounting for the effect of mycorrhization, possible solubilization of immobile P by root exudates, overestimation of the Michaelis constant (Km), and additional P uptake contributed by root hairs.

Many of the current plant models have been developed and designed based on the results from experiments conducted in containers with relatively limited width. This has caused the issue of the root architecture being skewed towards a narrow and deep spread of roots. Analysis of rice root growth in the field has shown the opposite: a large proportion of roots are concentrated in the topsoil (first 15 cm), even for upland rice genotypes (Wissuwa et al. 2020). This was not only due to extensive root branching in the topsoil layer but also to considerable extension of crown roots horizontally (Mori et al. 2016). It is therefore imperative that model parameterization be developed based on field data, and not just greenhouse data. We consider that the difference in root spread and depth seen from different experimental setups can be significant, as P concentrations in the topsoil are higher compared to deeper soil layers (Mori et al. 2016).

With this in mind, we believe that an assessment of the influence of S-types, root hairs, and general positioning of roots on P uptake is necessary.

The lack of an upland rice model including all fine structures and a root distribution pattern not affected by spatial limitations in root proliferation enticed us to develop such a model. We decided to base our model on the P efficient breeding line DJ123 for several reasons, namely that its root system had been characterized in several prior studies which showed DJ123 to be similar to other rice genotypes for many root traits (Mori et al. 2016; Nestler et al. 2016; Wissuwa et al. 2020); and that its efficient P uptake appears due to a combination of factors such as good early root vigor and high P uptake efficiency, rather than being caused by the extreme expression of a single root phenotype (Wissuwa et al. 2020).

**1.4 Thesis Objectives**

The objectives of our study were:

1) to obtain detailed data on root growth and P uptake of upland rice from both field and greenhouse experiments using DJ123 as a representative P-efficient upland rice genotype;

2) To use this data to parameterize and test a root architecture model that includes root hairs;

3) To use this root architecture model to simulate P uptake;

4) To conduct a sensitivity analysis in order to identify factors exerting a strong influence on P uptake;

5) To conduct a cost-benefit analysis with regard to P needed to grow a certain root class *versus* the P uptake provided by that class;

6) To integrate SWMS_3D into the model effectively and apply diverse environmental conditions to the model in order to take water presence in account for P uptake;

7) To use data obtained from environmental weathers stations, as well as measured soil data to parameterize atmospheric and soil conditions to simulate an accurate representation of P-deficient upland conditions;

8) To use diverse root angle distributions to simulate P uptake based on depth in order to identify strengths, weaknesses and overall effectiveness of said angle distributions when dealing with P-deficiency and drought conditions;

9) To integrate uptake-dependant modifications to growth and expansion into the model;

10) To use said model to predict growth and sizes of upland rice based on the type of soil and environmental conditions present.

**Chapter II: Cost-benefit analysis of the upland-rice root architecture in relation to phosphate: 3D Simulations highlight the importance of S-type lateral roots for reducing the pay-off time.**

## 2.1 Introduction:

For the last 30 years, bioinformatics has slowly taken a more prominent position in research, and is becoming much more important as stronger hardware becomes more accessible, opening for many possibilities and experiments previously thought impossible. Bioinformatics is a new and emerging science that combines the power of computers, mathematics algorithms, and statistics with concepts in the life sciences to solve biological problems.
Among the tools that came with the development of bioinformatics as a science, is modeling of living organisms as a whole. Of interest to us, are functional-structural plant models. Functional-structural plant models can be defined as models that combine the development of a 3D structure resembling a plant, as well as a representation of one or more physiological functions by means of mathematical equations in order to provide tools for researchers without having to rely on costly experiments. These models are a formal way to present quantitative knowledge about how a crop grows in interaction with its environment. Crop models can be used as a guide for breeding programs or as a means to envision a crop that we want to target or obtain. While simulation models can be used to predict appropriate trait phenotypes and selection protocols in breeding programs, for a true integration of crop models and breeding, a more detailed coordination between genetic research and modeling is required.

The objective is to develop a 3D root architectural model for the upland rice genotype DJ123, using root developmental parameters obtained by stepwise excavation of partial root systems of field grown plants or of entire seedling root systems from experiments conducted in containers large enough to not restrict root development of young plants.

## 2.2 Materials and Methods:

Root phenotyping experiments

Parameters to describe root architecture and development were obtained for the upland rice genotype DJ123 from field and greenhouse experiments conducted in Tsukuba, Japan, and described in detail in (Wissuwa et al. 2020). The soil was a highly P deficient (5 mg P $kg^{-1}$ soil, Bray-II) volcanic ash soil (Humic Haplic Andosol). Plants were sampled from the field at 8, 20, 28, 48, and 62 days after emergence (DAE) to count crown roots per plant, and at 28 and 48 DAE entire root systems were excavated up to a depth of 30 cm. During this process, individual roots were traced and their coordinates in terms of length from crown to root tip and depth of the root tip were recorded and used to calculate root growth angles. The absence of container size limitations in the field allowed us to trace roots horizontally for up to 50 cm from their origin at the crown. Excavated roots were stored in water in zipped freezer bags in a refrigerator at 4ºC until root scans were obtained. Shoots were dried and weighed as were roots after scans had been obtained. Tissue P analysis was done by digesting tissue samples in a 4:1 $HNO_3/HClO_4$ (nitric/perchloric) mixture followed by the determination of digest P concentrations in a microplate reader at 882 nm wavelength using the molybdenum blue assay defined by Murphy and Riley (1962).

A greenhouse experiment used the same field soil in containers of dimensions 23 x 46 x 15 cm depth (22-L) for harvests at 7 and 14 DAE or dimensions of 40 x 60 x 30 cm (72 L) for harvests at 21 and 28 DAE. Plants were sampled in weekly intervals by cutting off one side from the container and using a gentle water spray to remove the soil. This allowed us to excavate and scan intact root systems with minimum breakage. Afterward, the plants were treated and stored in the same manner as the excavated plants from the field experiments mentioned above.

Root scanning and analysis

Roots were spread out in a 20x25 cm Perspex tray filled with 0.5 cm of and scanned using an Epson Perfection V700 photo dual-lens scanner with top lighting, with the following settings: 600 dpi, 8-bit grayscale, positive film. Obtained images were analyzed by the WinRhizo software (Version 2008a, Regent Instruments Inc.) using a manual pixel classification with a gray-scale value of 225, to improve fine root detection. The debris filter was set to avoid counting debris with an area smaller than 1 $cm^2$, and a length/width ratio smaller than 5. The root system was divided into diameter classes of: 0-90 nm, 90-250 nm, 250-400 nm, 400-600 nm, 600-1000 nm, which correspond to S-type laterals (<90 nm), L-type laterals (90-250 nm) and crown roots (250-1000 nm). Details on branching frequencies or length of individual lateral roots were obtained using ImageJ as described by Wissuwa et al. (2020). Micrographs obtained with an Olympus DP21 microscope (Olympus, Tokyo, Japan) with an Olympus UPlanApo lens at 4x, 10x, 20x magnification were used to obtain exact measurements of root diameters.

Modeling root growth in OpenSimRoot

We chose the publicly available software OpenSimRoot git version 6f8e57d63f (Postma et al, 2017) to develop a 3D root growth model of genotype DJ123. The modular nature of OpenSimRoot allows the creation of mini-models (objects that encapsulate a state variable) that are combined into modules that form a major model component (e.g. root branching or phosphorus uptake). This allows users to easily add, remove, activate or deactivate components without having to rework the model in its entirety.

OpenSimRoot represents the root system by vertices and edges, with each root tip having its own vertex with dynamic coordinates, and as the root extends, vertices with fixed coordinates are placed behind it. Data required for this simulation are the location and time when root tips are created, the root growth rate, and the general direction of growth. In the initial step the primary root and hypocotyl emerge from the seed. Lateral roots emerge from parent roots depending on branching frequencies defined in space as an inter-branching distance (IBD) (Freschet et al. 2020). IBD is associated with the parent root class as the root tip of the parent root forms the primordia, whereas growth rates of laterals are defined by the lateral root class. Below, we summarize the main static and variable input parameters defining the root system development. For an extended explanation of the model, readers can refer to Postma et al. (2017).

- Rate of root primordia formation ($day^{-1}$): This variable is defined for crown roots as the rate at which their creation from the hypocotyl occurs, and is dependent on the time that has passed since the seed was planted.

- Inter-branching distances (IBD, cm) define the distance between one branching lateral root and the next. To account for varying lateral root densities, we modeled IBDs based on parent-root-specific distributions, using normal distributions (means and standard deviations derived from experimental data) with truncated tails defined by maximum and/or minimum values. The model computes the rate of primordia formation from the IBD, using the parent root elongation rate at the time the primordia was formed. Thus, faster growing roots form more primordia per time. IBD input parameters are given in supplementary Table S2. More frequent branching on the branched nodal roots was achieved manually through i) modifying the IBD distribution of fast nodal roots to roughly double the IBD during the initial 2 weeks of root development, and ii) to reduce subsequent branching frequencies since we observed that lateral root densities were higher in the basal half of the branched nodal roots.
- Growth rates (cm $day^{-1}$): These are defined depending on the time since a root was created or branched (in days). Each root class has its own growth rate derived from observations from weekly samplings in the greenhouse experiment. The growth rate is slower initially (root emergence), reaches a maximum 2-10 days after creation, and slows down thereafter. Each root received a multiplication factor pooled from a (log) normal distribution such that roots of the same class vary in growth rate and final length (see supplementary Table S3).
- General direction or growth: The initial growth direction is set by specified radial and axial branching angles. As the roots grow, the direction was changed by a tropism vector. The tropism vector is the combination of several vectors representing gravitropism, random impedance, and nutrient tropisms.
- Root diameter: The root diameters were set static for all root classes (0.065, 0.05, 0.06, 0.02, 0.0045 cm for primary and fast nodal roots, branched nodal roots, nodal roots of tillers, L-type and, S-type lateral roots, respectively).
- Specific root volume ($cm^3$ $g^{-1}$): It was assumed to be static, as senescence and cell apoptosis was not considered in this model. Values were derived from measured root biomass and corresponding root volume data of WinRhizo for the entire root system. Values used were 0.08 g $cm^{-3}$ for primary and nodal roots and this increased to 0.09 and 0.1 g $cm^{-3}$ for L-type and S-type lateral roots, respectively. This increase is reflecting the decreasing proportion of aerenchyma in fine roots and was supported by the observation of increasing specific root volume in root systems with a lower proportion of nodal roots.
- Tillering: Rice tillering was also implemented in the model and tillers will produce nodal roots originating from the lowest tiller nodes.

In modeling root growth, we made defined parameters for the following root classes:

- Primary root (more highly branched compared to nodal roots)
- Nodal root branched
- Nodal root fast (rapidly elongating nodal roots with less branching, increasing in frequency during later stages of development)
- Nodal roots of tillers (with a phenotype in between the other two nodal root classes)
- L-type lateral roots, with a distinction between branching off the primary root or nodal roots

- S-type lateral roots, with a distinction between branching off the primary root *versus* branching off nodal roots and L-type lateral roots.

Root hairs develop on each of the above root classes but with varying root hair length and density between i) primary root, ii) nodal and L-type lateral roots, and iii) S-type lateral roots (Nestler et al. 2016).

Making use of the modular nature of OpenSimRoot, we defined modules for growth of primary/nodal roots and L-type laterals, S-type laterals, and root hairs, and modules defining branching of L-type laterals, S-type laterals, and root hairs.

Root growth of genotype DJ123 was simulated over a 35-day period with a maximum timestep of 0.2 days for conditions of the highly P-fixing and therefore P deficient Andosol. Since P is considered the growth-limiting factor and since the root to shoot ratio is known to significantly increase in these conditions (Fageria et al. 2013; Wissuwa and Ae 2001), we did not model root growth in dependence of photosynthetic carbon resources but on the observed growth of P-deficient DJ123 (Wissuwa et al. 2020). The soil was assumed to have a homogeneous distribution of P.

Modeling P uptake in OpenSimRoot

A radial advection-diffusion-reaction model was used to simulate P uptake rates (µmol $cm^{-1}$ $day^{-1}$) at individual root vertices. P-uptake rates were integrated over the length of the root system and time to get the total P uptake by the plant (Silberbush & Barber, 1983 & 1984). P uptake is modeled for each individual root considering its length, radius, and presence of root hairs (at specific length and density). The soil parameters related to P availability were obtained based on analyses of the Andosol used in pot and field experiments and are summarized in supplementary Table S1 (Rakotoson, unpublished data). Simulations based on these values significantly underestimated measured plant P uptake, despite the inclusion of root hairs and S-type laterals (see introduction). We presume that rice roots can solubilize small amounts of P in the rhizosphere to achieve this but did not simulate the solubilization *per se* as data describing the relevant processes is not available. To simulate the correct P uptake, we instead changed the initial P concentration in the soil solution from the measured 83 nM to 540 nM, which is still very low. For the buffer power (b) we used a value of 6000 and the corresponding soil diffusion (De) was $9.227e^{-6}$ $cm^2$ $day^{-1}$ (supplementary Table S1).

Sensitivity analysis and model simulations:

A sensitivity analysis with five repeat runs was conducted with model base values altered by 25%, 50%, 100%, 150%, 200% and 400%. The analysis was conducted for two soil parameters (soil P concentration and buffer power) and six plant parameters: length and inter-branching distance for L-type and S-type roots, and length and density of root hairs. Effects of parameter variations on P uptake for a 28-day period were simulated.

We explored the cost-benefit aspects of different root classes. The weight of roots was calculated by the model as a function of root volume and specific densities of 0.06 g $cm^{-3}$ for nodal roots, 0.07 g $cm^{-3}$ for L-type roots, and 0.1 g $cm^{-3}$ for S-type roots and root hairs. Different specific volumes (cm3 /g) were assigned to root classes depending on the proportion of aerenchyma present in the respective class. The estimation of costs and benefits (P taken up) were simulated until day 31 (equal to 28 DAE in greenhouse/field experiments). Costs were estimated by multiplying

simulated root class weight times the average root P concentration of DJ123 at 28 DAE (0.8 mg $g^{-1}$). The cost recovery in days was estimated for three cases (see Table 3). In addition, simulations of cost-benefits were run for hypothetical root systems with shorter (0.5X) or longer (2.0X) S-type or L-type lateral roots and for reduced fast nodal root thickness (from 0.65 to 0.50 cm diameter).

**2.3 Results:**

DJ123 Rice Root Architecture:

Observations made during root excavations and in root scans led us to define 4 major root classes (primary root, crown roots, L-type and S-type laterals), of which nodal roots were divided into three subclasses we termed branched nodal roots, fast nodal roots (faster elongating and less branched compared to the branched nodal roots) and nodal roots forming on tillers (in-between fast and branched nodal roots). The primary root was observed to be the most densely branched root with the longest lateral roots (Figure 1). The first nodal roots developing were of the branched class, being of intermediate length (35 cm at 28 DAE) with a growth rate of up to 1.5 cm $day^{-1}$ and a root diameter between 340-650 μm (Table 1). Fast nodal roots started to develop between 7-14 DAE and increased in frequency as the root system matured. The length of the longest root excavated from the field at 28 DAE was 45 cm (Table 1). Assuming that the longest root was also the oldest one, we estimated it to be 21 days old and derived an average growth rate of 2.14 cm $day^{-1}$. The diameter of the fast nodal roots was larger compared to branched nodal roots, ranging from 550-850 μm.

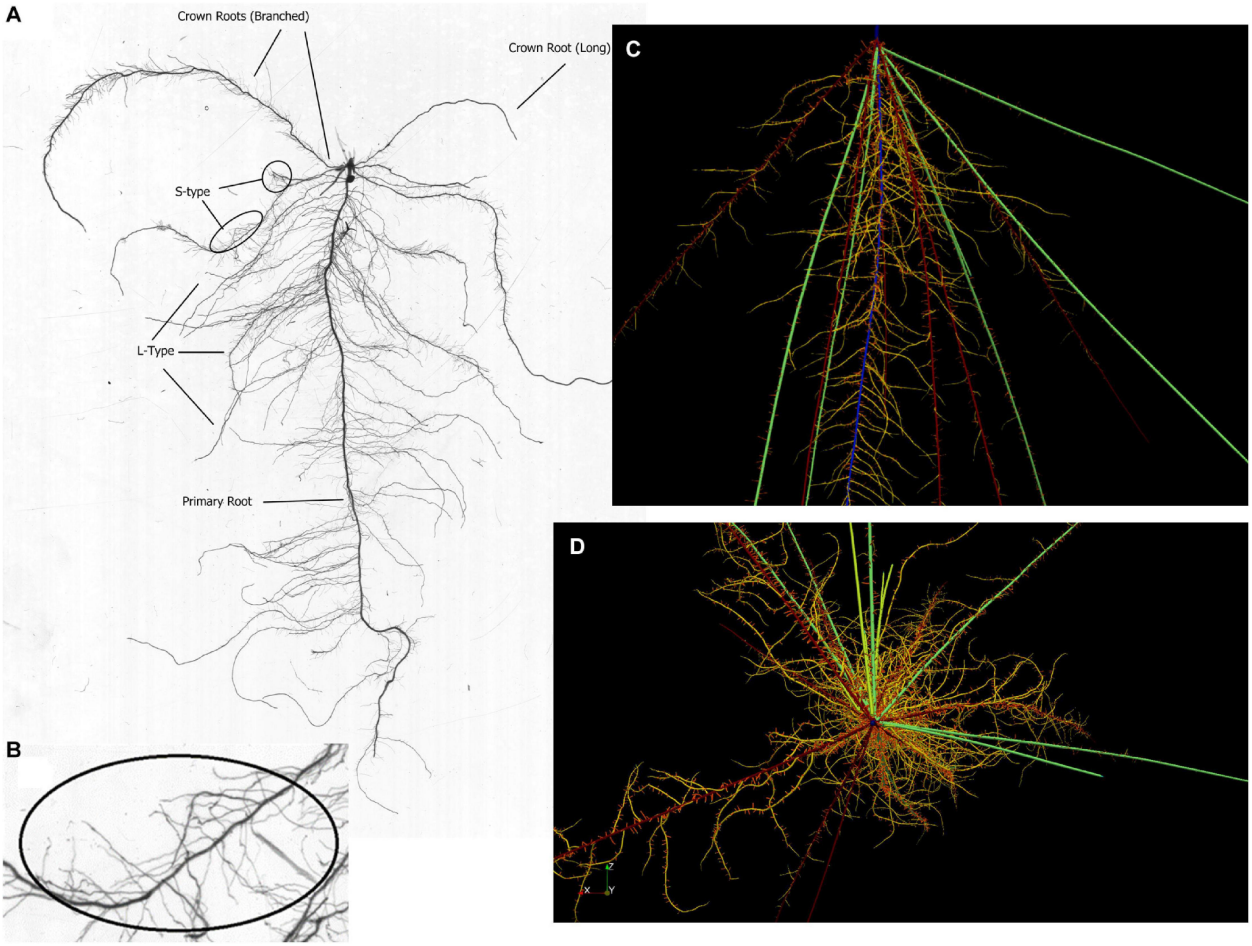


**Figure 1. (A)** Scan of a root system excavated 14 DAE from the greenhouse experiment showing the highly branched primary root as well as two nodal root classes and L-type and S-type lateral roots. Fast nodal roots start to develop between 7 and 14 DAE and therefore remain very small. **(B)** magnified region with a high density of S-type lateral roots. **(C)**Simulated root at 21 DAE where roots with their surrounding P depletion zones are shown for better visibility of lateral roots. Color coding identifies root classes: blue, primary root; dark red, branched nodal root; green, fast nodal root; yellow, L-type laterals; red, S-type laterals; light green, nodal roots from tillers. **(D)** Top-down view of a simulated root system at 28 DAE.

**Table 1:** Observed maximum root length, derived maximum daily growth rates and typical ranges of root diameters observed on primary, nodal and lateral roots. Data for nodal roots was obtained by tracing nodal roots horizontally (field experiment at 28 DAE). Data for primary and lateral roots was obtained by careful excavation of entire root systems before container size significantly restricted root development (greenhouse experiment at 21 DAE). Root hair parameters were adapted from Nestler et al. (2016).

| Root type | Maximum length | Estimated[x] growth rate | Diameter | Root hair density | Root hair length |
|---|---|---|---|---|---|
| | cm | cm $day^{-1}$ | µm | $cm^{-1}$ | cm |
| Primary root | 46 | 2.19 | 500-700 | 1400 | 0.02 |
| Nodal root (branched) | 35 | 1.46 | 340-650 | 1400 | 0.015 |
| Nodal root (long) | 45 | 2.14 | 550-850 | 1400 | 0.015 |
| L-Type root | 14.6 | 0.73 | 130-200 | 700 | 0.015 |
| S-Type root | 1.08 | 0.14 | 35-45 | 400 | 0.012 |

[x]Growth rates were estimated by dividing maximum length by root age. It was assumed that maximum length of all roots was achieved by the oldest of their class and that branched nodal roots formed from 2 DAE, fast nodal roots from 7 DAE, and L-type roots from 4 DAE.

Lateral roots varied in length and, presumably, in growth rates, with L-type and S-type lateral roots having developed on the primary root being 10% longer compared to roots from a branched nodal root. Similarly, root hairs were longer on the primary root (0.02 cm) compared to crown and L-type laterals (0.015 cm). Root hairs on S-type laterals were shorter (0.012 cm) and the maximum density was lower (400 hairs $cm^{-1}$) compared to L-type lateral (700 hairs $cm^{-1}$) and nodal roots (1440 hairs $cm^{-1}$). Based on observations by Nestler et al. (2016 b), it was assumed that the proportion of roots being alive is decreasing over time and this was modeled as a linear decreasing root hair density over time (e.g. from 600 hairs $cm^{-1}$ on a 3-day old root to 330 hairs $cm^{-1}$ on a 40-day old root).

Measurements of root length and depths, taken during excavations in the field at 28 DAE, provided data for root growth angles (RGA) of crown roots. These varied between 8 and 90 degrees (from the soil surface), with most roots having RGAs between 16-30° (Figure 2a; n=64). Overall, 62% of nodal roots had an RGA ≤ 45°. The distribution of RGAs appears to be steeper in Figure 2b than measured data would suggest (Figure 2a) but this is caused by roots growing towards the observer having been fully excavated and thereby losing their original root angle.

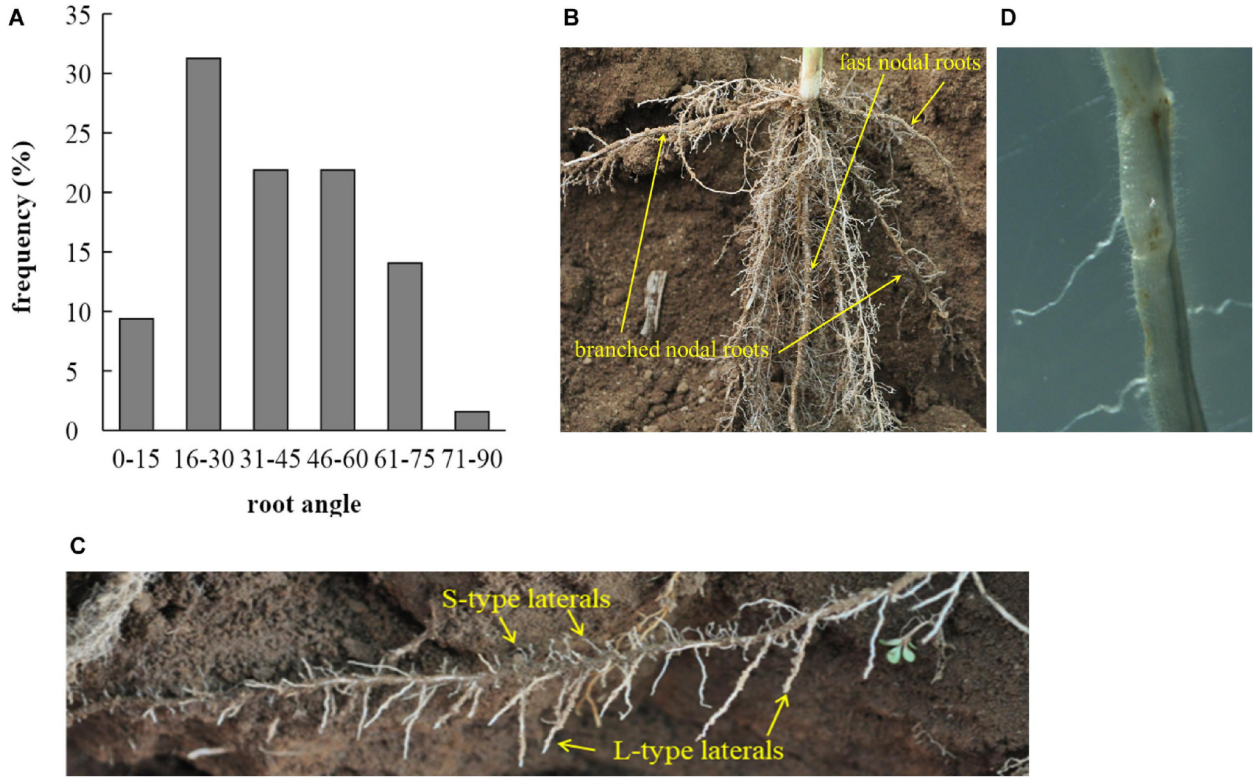


**Figure 2. (A)** Distribution of root growth angles (RGA, in degree from the soil surface) of nodal roots excavated 28 DAE from the field experiment and **(B)** partially excavated root system used to determine RGAs. The fast nodal roots are indicated in comparison to their branched counterparts. **(C)** A branched nodal root growing at a shallow angle developing a large number of L-type and S-type laterals. **(D)** Micrograph of an L-type lateral root section with S-type lateral roots and root hairs.

L-type and S-type lateral roots were assumed to develop perpendicular to their root of origin and their growth direction would therefore depend on where on the parent root they were initiated. The distribution of root development along the branched nodal root partially excavated from the field and shown in Figure 2c would suggest that the L-type lateral roots preferentially develop or extend on the downward side of nodal roots whereas S-type laterals appear as frequently on the upper half. This was simulated in OpenSimRoot by setting a boolean command named "cannotgrowup" which 'corrects' the growth direction of upwards growing roots to horizontal. The L and S type roots have no gravitropism modifier, whereas the primary root has a strong (-0.115 to -0.015 cm/cm/day) gravitropism, and crown roots a weak ( -0.0001 cm/cm/day) gravitropism.

Comparison of simulated and observed root growth of DJ123

The total root length (TRL) simulated by the model is the result of the various model inputs and shall thus be used to verify that simulated root system development is reflecting the observed root growth. The model slightly over-estimated TRL at 21 DAE and again at 48 DAE but was in-between the observed TRL from greenhouse and

field experiments at 28 DAE (Figure 3a). The biggest deviation form simulated total root length was seen in the field sample at 28 DAS and this may have been due to slower early root development in the field during the earlier part of the season when lower night-time temperatures may have limited growth. A main difficulty in modeling root development during the first 3-4 weeks stemmed from the observation that nodal root emergence was non-linear. Nodal root emergence was rapid during the first 7-10 days and this was followed by a slower increase in nodal root number during the next 7-10 days (Figure 3b). Thus, root development during the first 28 days neither followed a purely linear nor exponential growth trend. The model matched this initial slowdown (Figure 3b) by slowing the rate of nodal root formation from day 10. The slowing down might be associated with the depletion of seed reserves that supported rapid root development initially.

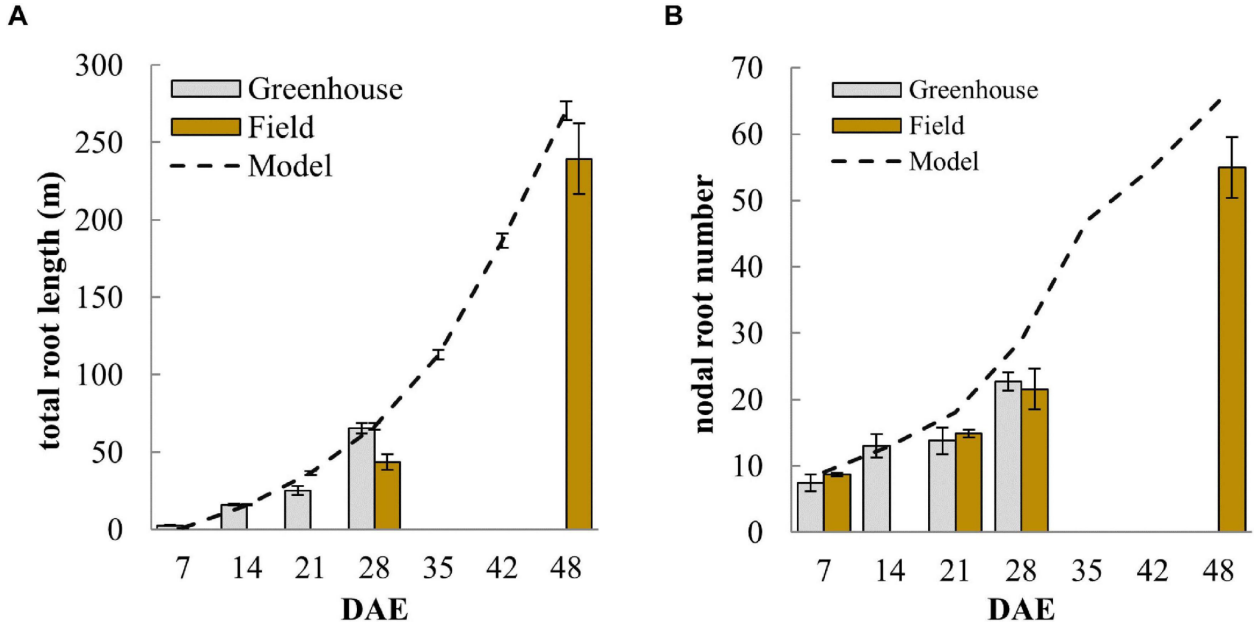


**Figure 3.** Development of **(A)** nodal root number and **(B)** total root length over time comparing measured values from greenhouse and field experiments with simulated data from the model. Error bars represent standard deviations (n = 4).

Simulation of root hairs and effects on total root length and P uptake

At 28 DAE the WinRhizo analysis of root scans indicated that about 61% of the total root length was contributed by S-type lateral roots, followed by 26% for L-type lateral and only 13% for nodal roots including the primary root (Figure 4 a). Modeled proportions were in general agreement, but L-type laterals had increased to 33.6% with ensuing minor reductions of other classes. Furthermore, simulations allowed us to compare the total length of root hairs to the length of the root system and individual root classes. The total length of all root hairs is 6.9-time the length of the root system. Root hairs on S-type lateral roots are short (0.12 mm) and present in lower density compared to L-type and nodal roots, nevertheless we estimated that 29.7% of the total root hair length is due to hairs on S-types (Figure 4 b). The proportion of total root hair length on L-type laterals is 38.7%. Hairs on all root classes combined have an estimated length of 482.3 m compared to 52.9 m for the actual roots. Due to the small diameter of

root hairs (5 µm) their contribution to total root surface area is only 13.3% (Figure 4 c). They only constitute 1.8% of total root volume (Figure 4 d).

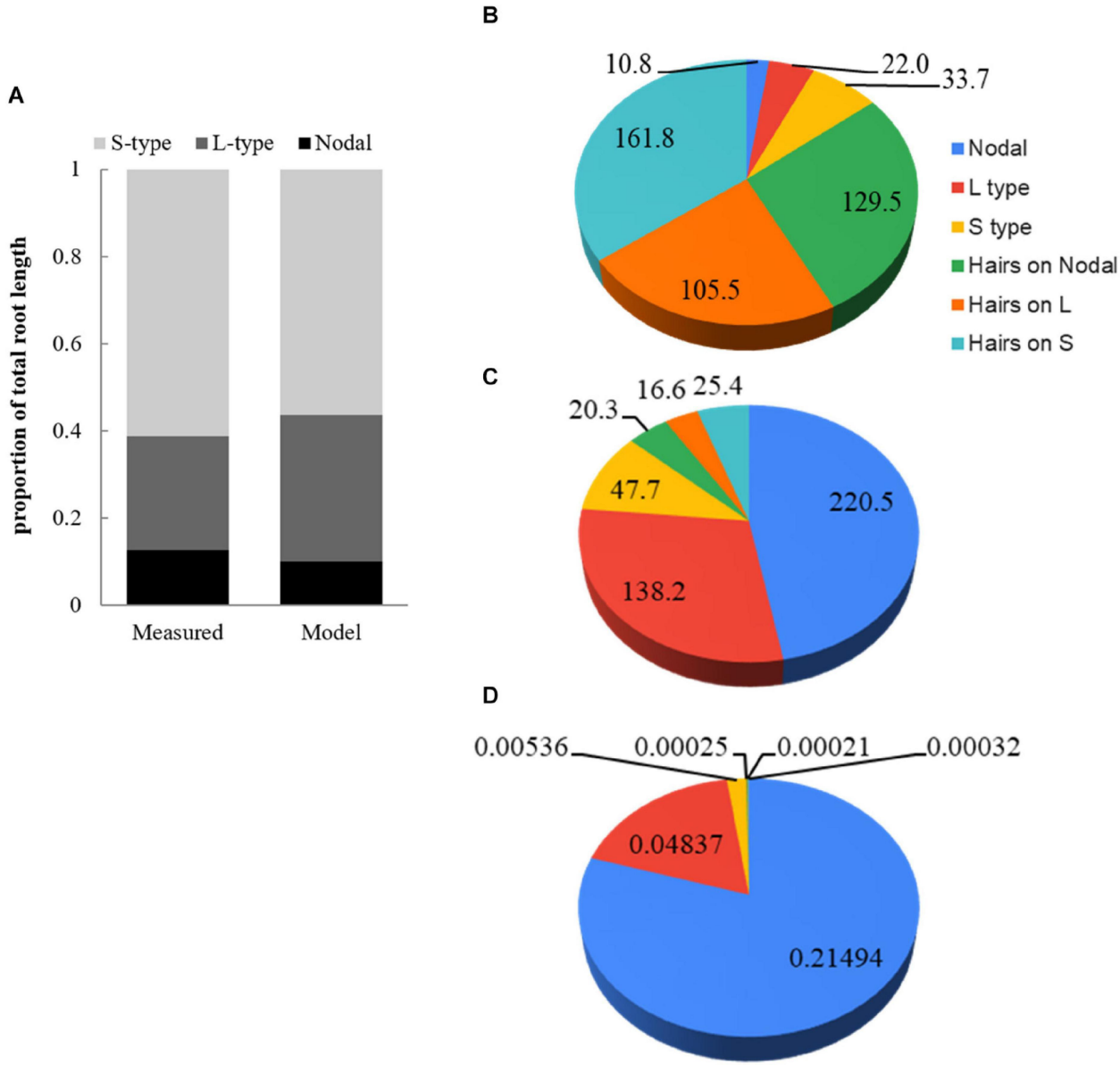


**Figure 4.** Comparison of root class distributions between **(A)** measured and model data and **(B)**modeled contribution (%) by root classes including root hairs developing on respective classes for total root length, **(C)**surface area, and **(D)**volume.

Simulation of P uptake

P uptake was initially modeled using the measured soil solution P concentration of 83 nM and that resulted in a plant P content of only 150.6 µg at day 28 (data not shown), compared to a measured P content of 774.3 µg. Such underestimation of P uptake under highly P deficient conditions is commonly observed in P uptake models,

indicating that more P is typically available to the plant than suggested by soil P extractions (Kirk et al. 1999). To account for the higher measured P uptake, we assumed that the roots, possibly through pH changes or some other rhizosphere modification, can solubilize P thereby increasing the P concentration in soil solution. Adopting a soil solution P concentration of 540 nM increased simulated P uptake to within standard deviations of measured P content at 21 and 28 DAE (Figure 5). All further simulations are using this higher soil P concentration in order to generate simulated P uptake that is comparable to observed uptake. However, even with this higher P concentration the model continued to underestimate P content in the field at 48 DAE (Figure 5) and this is because the P taken up per unit root length increased in the field to 26.2 µg P $m^{-1}$ from 12.1 µg P $m^{-1}$ at 28 DAE (Supplementary Figure S1). Respective values simulated by the advection-diffusion model implemented in OpenSimRoot were almost constant, only changing from 11.6 to 12.4 µg P $m^{-1}$ between 28 – 48 DAE.

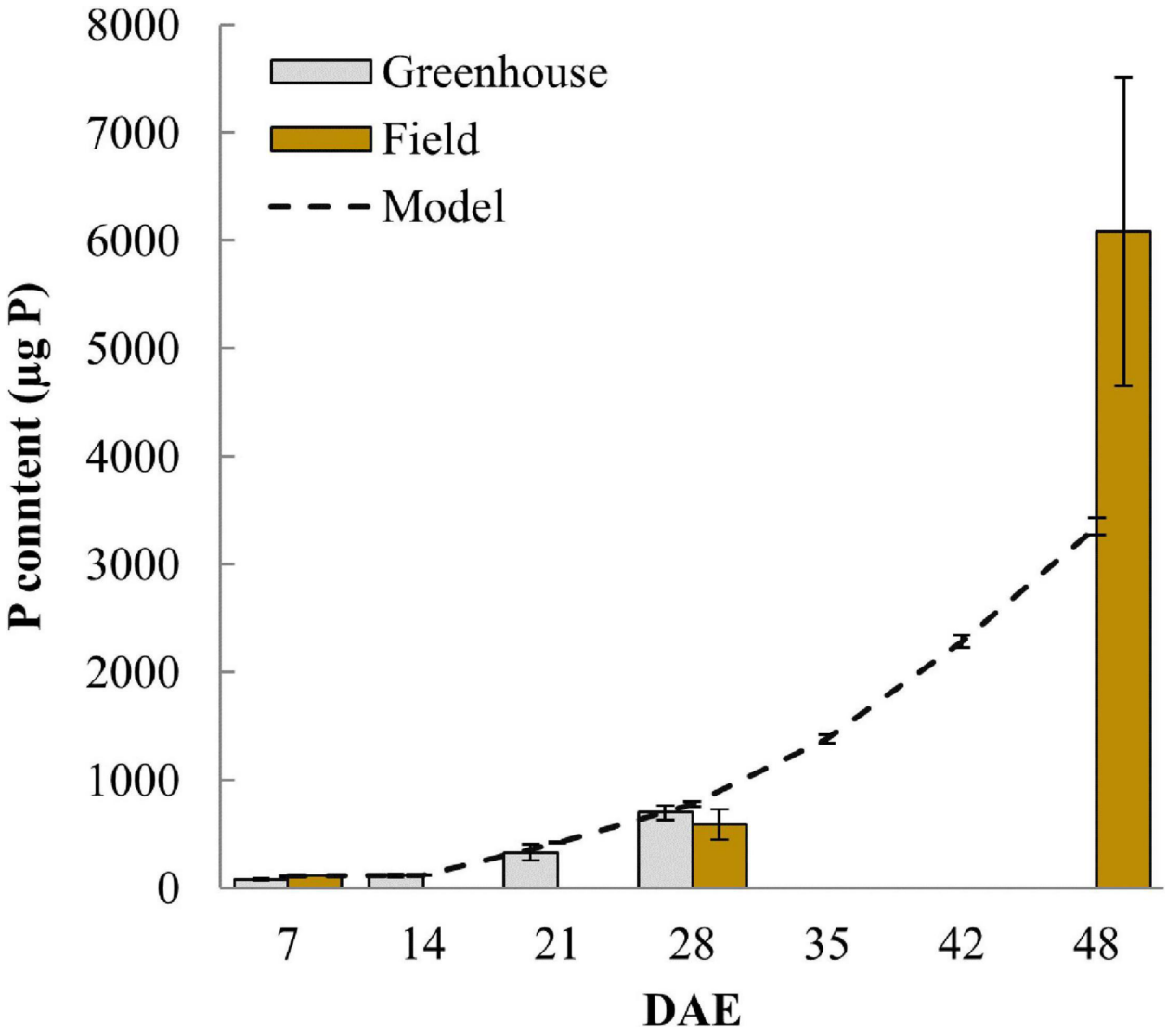


**Figure 5.** Plant P content over time comparing measured values from greenhouse and field experiments with simulated data from the model. Error bars represent standard deviations (n = 4).

Sensitivity analysis and cost-benefit simulations

The sensitivity analysis estimated to what extent P uptake was affected by changes in model input parameters. Variations in soil P concentrations across the entire 16-fold range from 25% to 400% showed a near-linear and proportional effect on P uptake (Table 2). Changes in soil buffer (b) and the corresponding changes in the diffusion coefficient (De) were less influential and seemed to be more sensitive to large increases than to proportionally large decreases. Effects of altering lateral root length and density were also assessed through changing the 'inter-branching distance' (IBD). Greater IBD leads to fewer lateral roots and, consequently, less uptake. Changes in lateral root length and density were more influential in L-type than S-type lateral roots and increasing L-type length was most effective in increasing P uptake (Table 2). The model was less sensitive to proportional decreases than to increases in lateral root length and density. Similar effects were detected for root hair length, but simulated P uptake was rather insensitive to changes in root hair density.

**Table 2**: Sensitivity analysis for two soil parameters (P concentration in soil solution and soil buffer power) and six root parameters (length and density for L-type roots, S-type roots, and root hairs). Parameters were varied by a factor 0.25X, 0.5X, 1.5X, 2.0X and 4X, with factor level 1 representing the base model. The sensitivity analysis estimated effects of parameter variations on P uptake for a 28 day period (25 DAE). Data shown are means of 5 repeat simulations.

| **P concentration in soil solution** | | | | **soil buffer power** | | |
|---|---|---|---|---|---|---|
| Factor level | P content (µg) | Change (%) | | Factor level | P content (µg) | Change (%) |
| 0.25 | 416 | 30 | | 0.25 | 866 | 62 |
| 0.5 | 732 | 53 | | 0.5 | 1071 | 77 |
| 1 | 1391 | 100 | | 1 | 1391 | 100 |
| 1.5 | 2029 | 146 | | 1.5 | 1622 | 117 |
| 2 | 2659 | 191 | | 2 | 1827 | 131 |
| 4 | 5087 | 366 | | 4 | 2738 | 197 |
| **L-type length** | | | | **S-type length** | | |
| Factor level | P content (µg) | change (%) | | Factor level | P content (µg) | change (%) |
| 0.25 | 947 | 68 | | 0.25 | 1160 | 83 |
| 0.5 | 1080 | 78 | | 0.5 | 1221 | 88 |
| 1 | 1391 | 100 | | 1 | 1391 | 100 |
| 1.5 | 1696 | 122 | | 1.5 | 1520 | 109 |
| 2 | 1995 | 143 | | 2 | 1678 | 121 |
| 4 | 3301 | 237 | | 4 | 2273 | 163 |
| **L-type branching distance** | | | | **S-type branching distance** | | |
| Factor level | P content (µg) | change (%) | | Factor level | P content (µg) | change (%) |
| 4 | 974 | 70 | | 4 | 1155 | 83 |
| 2 | 1100 | 79 | | 2 | 1230 | 88 |
| 1.5 | 1196 | 86 | | 1.5 | 1282 | 92 |
| 1 | 1391 | 100 | | 1 | 1391 | 100 |
| 0.5 | 1925 | 138 | | 0.5 | 1669 | 120 |
| 0.25 | 3042 | 219 | | 0.25 | 2232 | 161 |
| **root hair length** | | | | **root hair density** | | |

| Factor level | P content (µg) | change (%) | | Factor level | P content (µg) | change (%) |
|---|---|---|---|---|---|---|
| 0.25 | 1190 | 86 | | 0.25 | 1222 | 88 |
| 0.5 | 1215 | 87 | | 0.5 | 1278 | 92 |
| 1 | 1391 | 100 | | 1 | 1391 | 100 |
| 1.5 | 1624 | 117 | | 1.5 | 1481 | 107 |
| 2 | 1899 | 137 | | 2 | 1545 | 111 |
| 4 | 3168 | 228 | | 4 | 1804 | 130 |

When plant growth is directly limited by P availability, any new tissue produced incurs a cost in terms of P allocated to the respective tissue and this can be compared to the benefit this root provides in terms of P uptake. P uptake over a 28-day growth period was far higher in nodal roots compared to L-type and S-type lateral roots, and this was associated with the larger surface area nodal roots produced, despite having much lower total length (Table 3). Our simulations further showed that more than 80% of the total root system weight was due to nodal roots, which also meant that they contributed a similarly high share to the cost of a root system in terms of P invested. Root hairs on the other hand were negligible in terms of cost but increased P uptake by 19%, adding 22 % of extra surface area and 6-fold extra length (Table 3).

**Table 3**. Model simulation results by root class (and root hairs) showing root dimensions, costs in terms of P needed to produce roots, and benefits in terms of P taken up. Costs were estimated based on a P concentration of 0.8 mg $g^{-1}$ in all root classes including hairs. Data shown is for 31 days after germination (equivalent to 28 DAE in field and greenhouse experiments). The cost recovery in days was estimated for three cases. Case 1 is forward looking, estimating the time needed to recover the cost of a respective root class based on static costs and P uptake rates at 28 DAE. Case 2 and 3 are based on the cumulative costs and P uptake, starting at the time point a respective root class had emerged and simulating the days needed until cumulative P uptake has surpassed cumulative costs. For case 2 root hairs are included on the respective root classes whereas case 3 simulated P uptake without root hairs.

| | P | Total root | | | | P uptake efficiency | | | Benefit | Cost Recovery | | |
|---|---|---|---|---|---|---|---|---|---|---|---|---|
| | uptake | Length | Surface | Weight | Cost | Length | Surface | Weight | to cost | Case 1 | Case 2 | Case 3 |
| | µg | m | $cm^2$ | mg | µg P | µg $m^{-1}$ | µg $cm^{-2}$ | µg $mg^{-1}$ | ratio | days | days | days |
| Hairs | 110.0 | 395.9 | 62.2 | 0.78 | 0.6 | 0.3 | 1.77 | 141.4 | 176.8 | | | |
| S-type | 107.4 | 33.7 | 47.7 | 4.6 | 3.7 | 3.2 | 2.25 | 23.1 | 28.9 | 0.4 | 1.0 | 1.0 |
| L-type | 174.5 | 21.9 | 138.2 | 50.5 | 40.4 | 7.9 | 1.26 | 3.5 | 4.3 | 2.7 | 4.8 | 5.1 |
| Nodal | 297.4 | 10.8 | 220.5 | 399.9 | 319.9 | 27.6 | 1.35 | 0.7 | 0.9 | 12.5 | 24.8 | never |
| Total | 689.2 | 462.4 | 468.6 | 455.9 | 364.7 | 1.5 | 1.47 | 1.5 | 1.9 | | | |

When P uptake efficiency was estimated as P taken up per root length, main root axes were more efficient due to their larger diameter and surface area, however, per root weight finer roots and especially root hairs were far more efficient. When P uptake efficiency was estimated based on root surface area, root classes were rather similar with a slight efficiency advantage for S-type lateral roots. As a result of their very low cost, roots hairs had the best benefit to cost ratio, and we estimated that over the 31 day growth period, their cumulative P uptake exceeded their cost (P invested in producing them) by a factor 176.8 (Table 3). Based on the cost of a root class and the daily P uptake of that root class (static - both at 28 DAE) the number of days needed to recover that cost was estimated (Case 1, Table 3), suggesting that S-type lateral roots recover their own cost on the day of their emergence, whereas a nodal root

would require more than 12 days. Using a different cost-recovery scenario that estimates the break-even time point of a hypothetical developing root system made up entirely of one single root class puts nodal roots even more at a disadvantage relative to lateral roots (Case 2, Table 3). If one would simulate a root system without root hairs (Case 3) a continuously growing nodal root system would never reach the point where P uptake exceeds the P cost of producing the root system.

To test to what extent these large differences in benefit to cost ratio are affected by the model root parameterization, additional simulations were conducted with hypothetical root systems having reduced or increased S-type and L-type lateral root length or reduced nodal root diameter. Halving or doubling lateral root length had only minor effects on benefit-cost ratios (supplementary Table S4). More influential was a decrease in diameter of fast nodal roots (from 0.65 to 0.50 cm), offering over-proportionally high cost savings of 25% while lowering P uptake by only 8.2% (supplementary Table S4). While this meant nodal roots changed from a net-sink to a source of P, benefit-cost ratios of other root types remained several-fold higher.

**2.4 Discussion**

The potential utility of root architectural models in conceptualizing factors determining resource acquisition has long been recognized. Here our objective was to develop a 3D root architectural model for upland rice, using root developmental parameters obtained by stepwise excavation of partial root systems of field grown plants or of entire seedling root systems from experiments conducted in containers large enough to not restrict root development of young plants. A further step to simulate an upland rice root system as realistically as possible was the inclusion of root hairs as individual cylinders of given length and diameter, as opposed to simply expanding the overall radius of the parent root by the root hair length. Parameters of root hair length and density were adopted from Nestler et al. (2016 a b) who showed root hairs to exist even on S-type lateral roots. They furthermore showed root hair length to differ between root classes and to be substantially shorter in soil than in nutrient solutions. These findings have been included in the specification of root hair parameters for the first time in this model.

Modeling root development and 3D root architecture

Our model was able to simulate the root development of our model genotype DJ123 closely in terms of total crown roots or total root system length produced (Figure 3). The image presented in Figure 1 furthermore showed that crown roots developed at different angles from shallow to near-vertical. Our model estimated 87% of the roots to be present in the top 25 cm (data not shown) and this compares to 79% of root biomass in the top 25 cm detected in root excavations by Mori et al. (2016). Roots in that study were from 105-day old plants, which would have developed a higher proportion of deep roots compared to our simulated plant at 28 DAE.

In excavating roots we could visibly distinguish 2 classes of crown roots based on their thickness and the degree of branching. We have termed these branched and long nodal roots and to our knowledge such a distinction has not been made before. Nodal roots developing on young seedlings were of the branched class and as the plant matured, an increasing proportion of crown roots were of the faster and longer class. We hypothesized that such a change in predominant class is related to inter-root competition for resources as root zones may increasingly overlap closer to

the point of origin. Developing fast extending roots with little branching in the first 10 cm would be a way to limit placing resources in that overcrowded soil volume, however, model simulations did not support this hypothesis as overlapping depletion zones were found to be generally low and hardly affected by the presence or absence of the fast nodal root type (Supplementary Figure S2). Thus, the main advantage of rapidly extending roots into yet to be explored soil would presumably be to maximize exploration for water and nutrients and that fast nodal roots did not develop in young seedlings may simply be a reflection of their larger diameter which incurs a higher cost in terms of P and biomass. In combination with less branching it would take longer to recover that cost compared to branched crown roots and this could be more of a limiting factor in younger plants.

Modeling total P uptake over time

Using the extremely low measured soil P concentrations (0.083 nmol $mL^{-1}$) in modeling P uptake severely underestimated the actual measured P uptake in DJ123. Such underestimation is common in Barber-Cushman-based models if soil P availability is very low (Kirk et al. 1999), indicating that some processes that increase P availability, such as pH effects, root exudation, or soil microbial effects, are not properly accounted for in the model. We acknowledge that such processes should ideally be addressed in future models, but that is beyond the scope of the present study primarily focusing on contributions of different roots class to overall P uptake. We solved the underestimation of P uptake by increasing soil P concentrations to a level (540 nM) where P uptake matched observed uptake. While this may appear arbitrary, it allows us to model within the range of observed P uptake without making further assumptions about specific but untested P solubilization mechanisms.

The soil P concentrations used enabled us to closely match observed P uptake of field and greenhouse experiments up to 28 DAE, however, at 48 DAE field P uptake remained 81% higher compared to our modeled uptake. We hypothesize that this may be due to additional P provided through the arbuscular mycorrhiza (AM) pathway. Using the same soil Wissuwa et al. (2020) showed that roots of DJ123 and other rice genotypes started to be colonized by AM from 21 DAE onwards and that the symbiosis was active by 28 DAE without having contributed much additional P until then. It is likely that P provided through the AM pathway would increase with time in the field and may therefore add significantly to total plant P content at 48 DAE. If our hypothesis is true, at 48 days, as much as 40% of P uptake might have come from VAM. We note, however, that other mechanisms may contribute to additional P uptake as well, including slow release of P, mineralization of P, or solubilization through slowly changing rhizosphere pH.

Modeling P uptake by root class and cost-benefit analysis

In simulations of P uptake with and without root hairs present, we could estimate the contribution of root hairs and other root classes to P uptake. Most P (43%) is taken up by the nodal roots with L-type laterals also contributing substantially (25%), whereas S-type lateral roots and root hairs would only contribute around 15% each (Table 3). Their advantage becomes obvious, however, when P uptake is examined in relation to the cost of producing roots of a certain class. Due to their minute biomass, we estimated that root hairs have taken up 176-times more P than was necessary to construct them (at 28 DAE). P uptake to investment ratios were also high for S-type lateral roots and

simulating different root system architectures showed that the cost-benefit advantage of root hairs and S-type lateral roots over other root types was very consistent (supplementary Table S4). The high cost of producing nodal roots meant that their direct P uptake did not fully recover their cost. This could be reversed by reducing the crown root diameter, which incurred savings in terms of P cost that were greater than losses in P taken up. However, to what extent reduced crown root diameter would compromise water uptake needs to be considered. A slightly different way of evaluating cost and benefits would be to consider the cost recovery time. Despite some differences between cases 1 to 3, the common picture emerging from the cost recovery analysis was that low-cost S-type lateral roots and root hairs break even within one day, which would make them the root structure of choice for a root system adapted to P deficiency. The much later break-even point for crown root would furthermore explain why crown root number is very strongly reduced under P deficiency (Wissuwa et al. 2020).

Optimizing the root system

A question of practical relevance in plant breeding is related to the choice of traits to be targeted in selection in order to maximize varietal performance. In the context of the present study one may explore different root classes and their properties as likely targets for selection. The sensitivity analysis identified L-type lateral root length and root hair length as the two most influential parameters. That the length of L-type lateral roots was more influential compared to S-type length was likely due to the fact that longer L-types automatically produce more S-type laterals, assuming a constant branching frequency of S-types on L-types. This would be consistent with the conclusion by De Bauw et al (2020) that total P uptake was dependent on the number of total root tips, which in turn depends on the rate of secondary branching on L-type laterals. Thus, producing higher-order roots would seem advantageous due to the knock-on effect on increasing subsequent roots classes and root hairs. However, the cost-benefit analysis indicated higher-order roots are less effective per P invested, which would favor the formation of root hairs and S-type lateral roots as traits for better adaptation to more severe P deficiency. This would also hold true in relation to cost per root tip as S-type roots are by far the most numerous root type. A point to be addressed in future studies is to what extent the process of continuous root tip growth into yet unexplored soil is crucial (De Bauw et al. 2020), as S-type roots will reach their maximum length of around 1 cm faster compared to longer L-type laterals.

The sensitivity analysis showed that increasing the length of root hairs was far more beneficial for P uptake compared to increasing root hair density. Employing a very different modeling approach Zygalakis et al. (2011) reached the same conclusion. Should root hair length therefore be a primary target trait in rice improvement? This depends to what extent genotypic differences in root hair extension will be realized in soil. Nestler et al. (2016 a) reported average root hair length of 430 µm on nodal roots grown in low-P nutrient solution, which decreased to below 200 µm on soil-grown roots. In-situ synchrotron images of a soil-grown root with 243 visible root hairs furthermore clarified that a maximum length of 395 µm could be reached by hairs developing into larger soil pores, but that the average length of root hairs was a mere 122 µm due to the physical barrier imposed by soil particles (Nestler et al. 2016 a) and the inability of hairs to bend and grow around obstacles. Thus, a crucial question to be resolved is to what extent potential genotypic differences in root hair length would be realized in the field and whether genotypic differences in the ability to extend root hairs against soil resistance exist.

Unlike root hairs, S-type lateral roots can modify their growth direction (see Figure 2 d) and can therefore elongate around soil particles, and selection for increased S-type length would be the second-most efficient way to increase P uptake per cost. To our knowledge, efforts to systematically evaluate genotypic differences in S-type lateral root length have not been made. One interesting aspect of our cost-benefit analysis regarding S-type lateral roots is that they become a net-source of P after only one day of existence, much earlier compared to larger root classes. What remains unknown is for how long these S-type roots remain active and contribute to uptake of P and other resources. Their relative advantage would diminish if their active life span was very limited and further investigations clarifying this point are needed. As for S-type length, any genotypic difference in longevity would potentially be worth exploiting in rice breeding.

## Conclusions

We constructed a detailed model of the root architecture and morphology of upland rice, using DJ123 as a representative of upland rice genotypes with adaptations to low P soils. Modeling its root system with S-type lateral roots more than doubled root system length and adding root hairs further increased total length several-fold. Despite the presence of such extensive length in fine structures, P uptake attributable to these structures was only around 30% because the corresponding surface area was small. The significance of the fine root structures characterizing an upland rice root system appear to be related to their low cost. Under severe P deficiency root growth is reduced, presumably by the growth-limiting factor P. P invested in extending a root system therefore represents a crucial cost and the rapid recovery of that cost by S-type lateral roots and root hairs may enable rice to continuously expand its root system, thereby maintaining P uptake.

**Chapter III: Cost-benefit analysis of the upland-rice root architecture in relation to phosphate: 3D Simulations highlight the importance of angle distributions for P uptake in drought conditions.**

As the contents of this chapter are anticipated to be published in a paper in a scholarly journal, they cannot be published online. The paper is scheduled to be published within 1 year.

**Chapter IV: Phosphorus Deficiency Stress Effects on Plant Growth: Plant Functional-Structural Models aid in the Determination of Optimal Nutrient Concentrations for Growth.**

As the contents of this chapter are anticipated to be published in a paper in a scholarly journal, they cannot be published online. The paper is scheduled to be published within 1 year.

## Chapter V: Conclusions and looking forward

**Results:**

During the course of this research, we concluded that it is indeed possible to model upland rice to an adequate degree of fidelity compared to the field plants.

Using models is a good way of obtaining data that can be hard to measure, or close to impossible to obtain through normal experimentation. Most, if not all of the results shown here would be extremely difficult or unreliable to measure in the field or even in laboratory conditions.

There is however, the necessity to obtain precise data; the better and more detailed the starting plant and environment data, the more accurate the model will be at simulating close to reality.

When simulating upland rice, we determined through the use of modeling techniques, the effectiveness of P uptake per root, the effectiveness of each root class for taking up P in terms of length, surface area, and volume, as well as making calculations about the time required for replenishing the expenditure of P utilized to produce said roots. We also determined the effectiveness of root uptake per layers of depth and analyzed the effectiveness of deeper root plants vs shallow root plants in case of P deficient soils, and determined in which cases deeper roots would be preferred against shallower roots and vice-versa.

We also were able to upgrade the model to be usable in more different conditions and have it react properly to deficiencies, making it lower its growth rates and change expansion rates depending on the predicted nutrient intakes.

**Future Prospects:**

While the models have been pretty effective at what they are currently being used for, there is still much room for upgrades for these upland rice models. Currently the model is only able to create 3D architecture and details calculations for roots, with relatively coarse shoot design and calculations. However, modifications can be done with some work in order to more effectively simulate shoot mechanics, if this were to be of interest.

Our emphasis in this research was P uptake mechanics, due to it being the focus of the ongoing research in the laboratory. The groundwork and code is already in place for other nutrient considerations, such as nitrogen, potassium or even carbon uptake and usage mechanics. They can be used to quantify uptake as was done in this research, or in conjunction with each other. However, the more complex the model, the greater the amount of calculations the program requires due to interactions between modules. This can mean a very steep slope in calculation time and hardware necessities. Care must be taken to make sure the modules activated are actually required for the objectives. Modifications to code and reductions in resolution can fix these issues, however the accuracy of the data obtained can suffer as a result.

That the model currently requires a small, but reasonable awareness of computational knowledge has been our concern for some time. While the level in order to operate it basically can be easily acquired in a small amount of time, any more complex edits and modifications require a bit more knowledge and time. This can make it a bit unwieldly for researchers who just want to use it sparingly. The addition of a GUI (Graphical User Interface) that hides all the fragile code and displays numbers and other data in a user-friendly way would be a very welcome addition as well.

As a final consideration, while this research was heavily focused mostly on upland rice, all the improvements and QOL (Quality of Life) modifications can be easily moved to other plants, as long as basic data about them has been obtained. After all, the base engine for the model was designed for other plants initially and was later adapted for use for rice.

**Supplementary material**

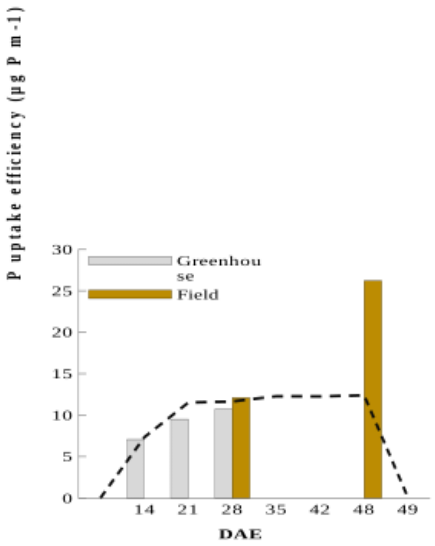


**Supplementary Figure S1** Estimated P uptake efficiency (P taken up per unit of root length) over time comparing values from greenhouse and field experiments with simulated data from the model. Error bars represent standard deviations (n=4 for experimental data).

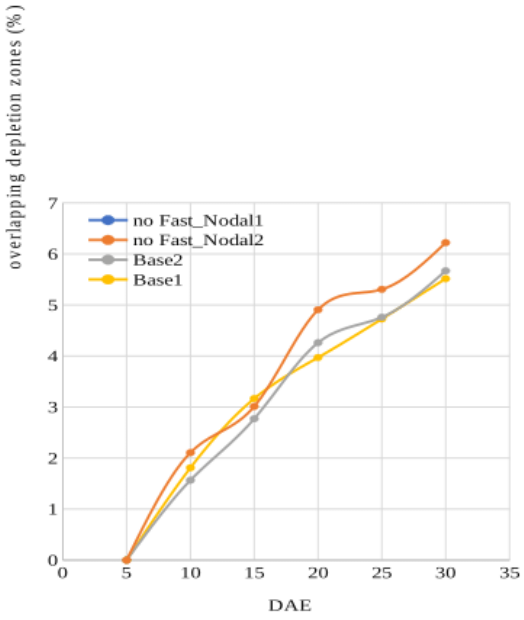


**Supplementary Figure S2** Estimation of overlapping depletion zones, comparing the base model with a simulation replacing the fast nodal roots with branched nodal roots.

| supplementaryTable S1 Soil parameters used in the model based on analyses by Rakotoson (unpublished) | | |
|---|---|---|
| P concentration in soil solution | 83 | nM |
| Soil Diffusion (De) | 0.00000922752 | $cm^2\ day^{-1}$ |
| Buffer Power (b) | 6000 | $Dm^3$ |
| Adsorption Coefficient () | 1333.3 | $\mu mol\ cm^{-1}$ |
| Saturated Diffusion Coefficient () | 0.00495 | $cm^2\ day^{-1}$ |

| | | |
|---|---|---|
| H2PO4-Diffusion coefficient in water (Di) | 0.7344 | $cm^2\ day^{-1}$ |
| Soil volumetric Water Content (θ) | 0.3 | $Dm^3$ |
| Diffusion impedance factor (tortuosity factor) (f) | 0.2 | N/A |

Table A: IBD input parameters for the root structure branching.

| Root Class | | | |
|---|---|---|---|
| | Growth Rate Calculation type: | Modifier | Additional Modifier |
| Primary Root Branching (L-type) | Table 2 | Normal | Yes |
| Primary Root Branching (S-type) | Table 3 | Normal | No |
| S-type Branching in Other Roots | Table 4 | Normal | No |
| L type Branching on Nodal Root (Fast) | Table 5 | Normal | No |
| L type Branching on Nodal Root (Branched) | Table 6 | Normal | No |
| L type Branching on Nodal Roots of tillers | Table 7 | Normal | No |

Table A shows the index of IBD imput parameters for each type of root.

Tables 2 to 7 show the interbranching distance per days of creation, as well as any modifiers that affect them.
The Branching Frequency represent the IBD between the roots branching from a specific root.
In the case of the L-type branching in Primary roots, there is a multiplier applied to add the stochastisity to a base IBD.
S-type IBD is modeled to be consistent across the root structure except for the primary root.

Table 3: L-type branching in Primary Root

| L-type Laterals: | | |
|---|---|---|
| Branch Emergence Delay: | 1 | day |
| Branch Spatial Offset: | 1.5 | cm |

| Branching Frequency | | Frequency Multiplier | |
|---|---|---|---|
| day | cm | | |
| 0 | 0.25 | Type: | Normal |
| 10 | 0.25 | Mean: | 1 |
| 16 | 0.4 | Stdev: | 0.3 |
| 28 | 0.4 | min: | 0.15 |
| 40 | 1 | Max: | 2 |
| | | Unit: | N/A |

Table 4: S-type branching in Primary Root

| S-Type Laterals: | | |
|---|---|---|
| Branch Emergence Delay: | 1 | day |
| Branching Frequency: | | |
| Type: | Normal | |
| Mean: | 0.15 | |
| Stdev: | 0.03 | |
| min: | 0.1 | |
| Max: | 0.5 | |
| Unit: | Cm | |

Table 5: S-type branching for other roots

| S-Type Laterals: | | |
|---|---|---|
| Branch Emergence Delay: | 1 | day |

| | |
|---|---|
| Branching Frequency: | |
| Type: | Normal |
| Mean: | 0.18 |
| Stdev: | 0.03 |
| min: | 0.1 |
| Max: | 0.5 |
| Unit: | Cm |

Table 6: L-type Laterals In Fast Nodal Roots:

| L-type Laterals In Fast Nodal Roots: | | |
|---|---|---|
| Branch Emergence Delay: | 2 | day |
| Branch Spatial Offset: | 8.5 | cm |
| Branching Frequency: | | |
| Type: | Normal | |
| Mean: | 1 | |
| Stdev: | 0.1 | |
| min: | 0.5 | |
| Max: | 2 | |
| Unit: | Cm | |

Table 7: L-type Laterals in Branched Nodal Roots:

| L-type Laterals: | | |
|---|---|---|
| Branch Emergence Delay: | 1 | day |
| Branch Spatial Offset: | 2 | cm |
| | | |
| Branching frequency | | |
| Type: | Normal | |
| Mean: | 1 | |
| Stdev: | 0.2 | |
| min: | 0.2 | |
| Max: | 2 | |
| Unit: | Cm | |

Table 8: L-type Laterals In Nodal Roots of Tillers:

| L-type Laterals: | | |
|---|---|---|
| Branch Emergence Delay: | 1 | day |
| Branch Spatial Offset: | 2 | cm |
| | | |
| Branching frequency | | |
| Type: | Normal | |
| Mean: | 1 | |
| Stdev: | 0.2 | |
| min: | 0.2 | |
| Max: | 2 | |
| Unit: | Cm | |

Table B: Root Growth Imput Parameters

| Root Class | Growth Rate Calculation type: | Additional Modifier | Additional Modifier |
|---|---|---|---|
| Primary Root | Table 8 | None | No |
| Nodal Root (fast) | Table 9 | Lognormal | Yes |
| Nodal Root (Branched) | Table 10 | Lognormal | Yes |
| Nodals of Tillers | Table 11 | Lognormal | Yes |
| L-type (primary) | Table 12 | Lognormal | Yes |
| L-type (Nodals) | Table 13 | Lognormal | No |
| S-type (primary) | Table 14 | Lognormal | No |
| S-type (Nodals) | Table 15 | Lognormal | No |

Table 8 shows the index of root growth imput parameters for each type of root.

Table 8 Growth rate primary root (cm $day^{-1}$)

Primary Root Table:

| day | cm day-1 |
|---|---|
| 0 | 0.01 |
| 1 | 1.8 |
| 2 | 2.2 |

| | |
|---|---|
| 10 | 1.9 |
| 55 | 1.5 |

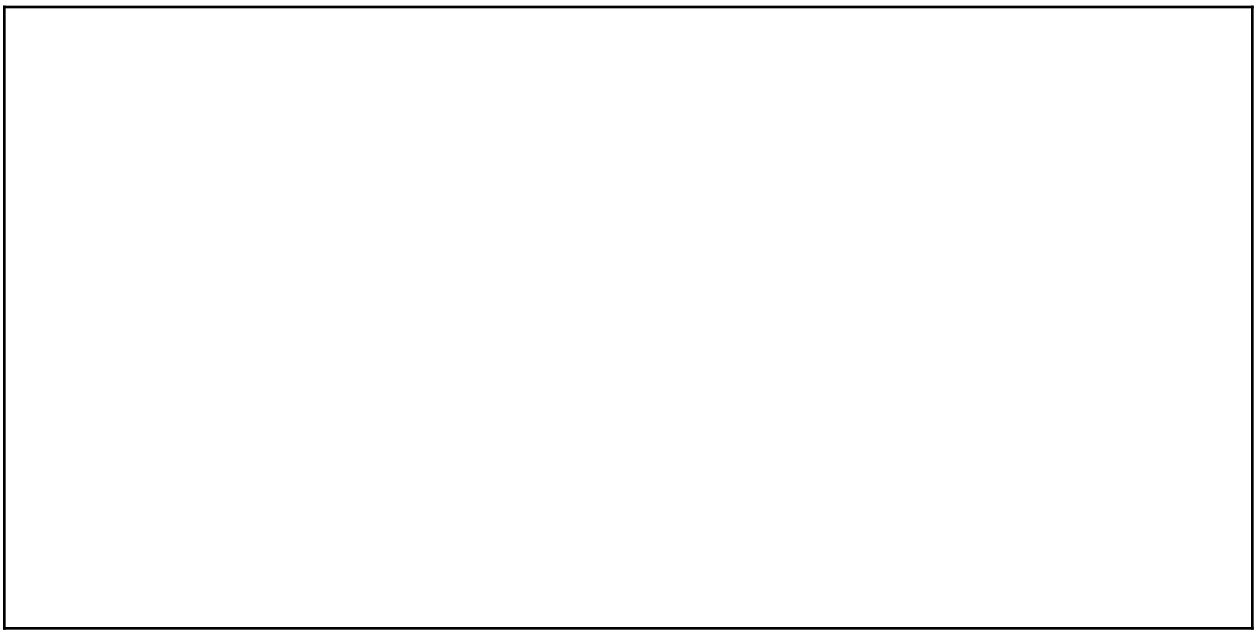

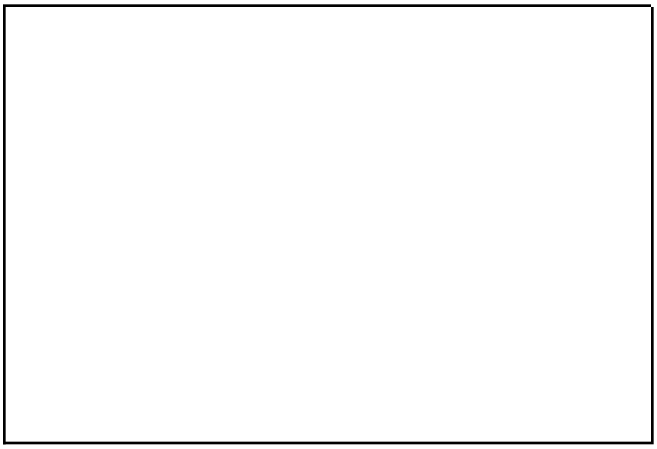

Tables 9 to 15 represent the growth rates per day of the roots at a given timepoint in the simulation.

Longitunidal multipliers, if given, represent a multiplier that affects the base growth rate given in the table.

Ocasionally, there may exist more than one multiplier affecting a root.

Table 9 Growth rate Nodal Root (fast) (cm day$^{-1}$) and modifiers

| Nodal Root (fast) Table: | | Longitudinal Multiplier: | | Length to Diameter Multiplier | |
|---|---|---|---|---|---|
| day | cm day-1 | | | | |
| 0 | 0.01 | Type: | Lognormal | | |
| 1 | 1 | Mean: | 1.5 | 0 | 0 |
| 2 | 2.2 | Stdev: | 0.3 | 1 | 1.1 |
| 14 | 2 | min: | 0.8 | 10 | 10.2 |
| 25 | 1.9 | Max: | 2 | | |
| 35 | 1.5 | Unit: | Cm | | |
| 65 | 0.0001 | | | | |

Table 10 Growth rate Nodal Root (branched) (cm day$^{-1}$) and modifiers

| Nodal Root (branched) Table: | | Longitudinal Multiplier: | | Length to Diameter Multiplier | |
|---|---|---|---|---|---|
| day | cm day-1 | | | | |
| 0 | 0.01 | Type: | Lognormal | | |
| 1 | 1 | Mean: | 1.3 | 0 | 0 |
| 2 | 2 | Stdev: | 0.2 | 1 | 1 |
| 14 | 1.9 | min: | 0.8 | 10 | 10 |
| 25 | 1.8 | Max: | 2 | | |
| 35 | 1.6 | Unit: | Cm | | |
| 65 | 0.0001 | | | | |

Table 11 Growth rate Nodal Roots of Tillers (cm day-1) and modifiers

| Nodal Root of Tiller Table: | Longitudinal Multiplier: | Length to Diameter Multiplier |
|---|---|---|

| day | cm day-1 | | | | |
|---|---|---|---|---|---|
| 0 | 0.01 | Type: | Lognormal | 0 | 0.5 |
| 1 | 1 | Mean: | 1 | 0.7 | 0.8 |
| 2 | 2.1 | Stdev: | 0.011 | 1 | 1 |
| 15 | 1.8 | min: | 0.7 | 2 | 1.2 |
| 25 | 1.7 | Max: | 4 | 4 | 1.3 |
| 35 | 1.6 | Unit: | Cm | 10 | 1.3 |
| 65 | 0.0001 | | | | |

Table 12 Growth rate of L-types on Primary root (cm day-1) and modifiers

| L-type (Primary) Table: | | Longitudinal Multiplier: | |
|---|---|---|---|
| day | cm day-1 | | |
| 0 | 0 | Type: | Lognormal |
| 3 | 0.5 | Mean: | 1 |
| 4 | 0.5 | Stdev: | 0.3 |
| 8 | 0.4 | min: | 0.5 |
| 10 | 0.3 | Max: | 2 |
| 17 | 0.2 | Unit: | Cm |
| 21 | 0.2 | | |
| 23 | 0.2 | Longitudinal Multiplier: | |
| 25 | 0.2 | | |
| 30 | 0.2 | 0 | 1.3 |
| | | 6 | 1 |
| | | 10 | 0.9 |

Table 13 Growth rate of L-types onNodal roots (cm day-1) and modifiers

| L-type (nodal) Table: | | Longitudinal Multiplier: | |
|---|---|---|---|
| day | cm day-1 | | |
| 0 | 0 | Type: | Lognormal |
| 3 | 0.4 | Mean: | 1 |
| 4 | 0.4 | Stdev: | 0.3 |
| 8 | 0.3 | min: | 0.5 |
| 10 | 0.3 | Max: | 2 |
| 17 | 0.2 | Unit: | Cm |
| 21 | 0.2 | | |
| 23 | 0.2 | | |
| 25 | 0.2 | | |
| 30 | 0.2 | | |

Table 14 Growth rate of S-types on Primary root (cm day-1) and modifiers

| S-type (Primary) Table: | | Longitudinal Multiplier: | |
|---|---|---|---|
| 0 | 0 | Type: | Lognormal |
| 1 | 0 | Mean: | 1.2 |
| 2 | 0.1 | Stdev: | 0.3 |
| 4 | 0.1 | min: | 1 |
| 5 | 0 | Max: | 2 |
| | | Unit: | Cm |

Table 15 Growth rate of S-types on Nodal roots (cm day-1) and modifiers

| S-type (nodal) Table: | Longitudinal Multiplier: |
|---|---|

| | | | |
|---|---|---|---|
| 0 | 0 | Type: | Lognormal |
| 1 | 0 | Mean: | 1.2 |
| 2 | 0.1 | Stdev: | 0.1 |
| 3 | 0.1 | min: | 0.9 |
| 5 | 0 | Max: | 1.5 |
| | | Unit: | Cm |

Supplementary Table 4: Group of tables showing cost vs benefit calculations with different values (0.5x and 2.0x) for lengths in S-types, L-types, and a change in nodal root diameter.

Base

| Root Type | P uptake (ug) | RL (m) | RWt (mg) | RE-L (ug/m) | RE-Wt (ug/mg) | Cost | (µg P) | Benefit/ cost | Benefit/cost vs Base | Cost Recovery |
|---|---|---|---|---|---|---|---|---|---|---|
| Root Hair | 109.99 | 395.90 | 0.78 | 0.28 | 141.44 | 0.62 | | 176.79 | 100.00 | 0.07 |
| S-type | 107.35 | 33.70 | 4.64 | 3.19 | 23.14 | 3.71 | | 28.93 | 100.00 | 0.40 |
| L-type | 174.50 | 21.98 | 50.52 | 7.94 | 3.45 | 40.42 | | 4.32 | 100.00 | 2.70 |
| Nodal Roots | 297.36 | 10.79 | 399.97 | 27.56 | 0.74 | 319.98 | | 0.93 | 100.00 | 12.53 |
| total | 689.21 | 462.38 | 455.91 | 1.49 | 1.51 | 364.73 | | 1.89 | 100.00 | 6.16 |

S-type lateral length x 0.5

| Root Type | P uptake (ug) | RL (m) | RWt (mg) | RE-L (ug/m) | RE-Wt (ug/mg) | Cost | (µg P) | Benefit/ cost | Benefit/cost vs Base | Cost Recovery |
|---|---|---|---|---|---|---|---|---|---|---|
| Root Hair | 88.82 | 315.10 | 0.62 | 0.28 | 143.50 | 0.50 | | 179.38 | 101.46 | 0.06 |
| S-type | 53.41 | 16.81 | 2.32 | 3.18 | 23.01 | 1.86 | | 28.76 | 99.43 | 0.38 |
| L-type | 174.14 | 21.95 | 50.55 | 7.93 | 3.45 | 40.44 | | 4.31 | 99.74 | 2.56 |
| Nodal Roots | 298.48 | 10.76 | 395.43 | 27.75 | 0.75 | 316.34 | | 0.94 | 101.53 | 11.70 |

| | | | | | | | | | |
|---|---|---|---|---|---|---|---|---|---|
| total | 614.84 | 364.62 | 448.92 | 1.69 | 1.37 | 359.13 | 1.71 | 90.60 | 6.45 |

S-type lateral length x 2.0

| Root Type | P uptake (ug) | RL (m) | RWt (mg) | RE-L (ug/m) | RE-Wt (ug/mg) | Cost (µg P) | Benefit/ cost | Benefit/cost vs Base | Cost Recovery |
|---|---|---|---|---|---|---|---|---|---|
| Root Hair | 137.65 | 557.20 | 1.09 | 0.25 | 125.76 | 0.88 | 157.21 | 88.92 | 0.07 |
| S-type | 217.51 | 67.23 | 9.25 | 3.24 | 23.50 | 7.40 | 29.38 | 101.57 | 0.36 |
| L-type | 173.63 | 21.92 | 50.36 | 7.92 | 3.45 | 40.28 | 4.31 | 99.82 | 2.44 |
| Nodal Roots | 297.60 | 10.77 | 396.58 | 27.63 | 0.75 | 317.26 | 0.94 | 100.93 | 11.20 |
| total | 826.38 | 657.13 | 457.28 | 1.26 | 1.81 | 365.83 | 2.26 | 119.54 | 4.65 |

L-type lateral length x 0.5

| Root Type | P uptake (ug) | RL (m) | RWt (mg) | RE-L (ug/m) | RE-Wt (ug/mg) | Cost (µg P) | Benefit/ cost | Benefit/cost vs Base | Cost Recovery |
|---|---|---|---|---|---|---|---|---|---|
| Root Hair | 72.91 | 290.85 | 0.57 | 0.25 | 127.62 | 0.46 | 159.52 | 90.23 | 0.07 |
| S-type | 76.21 | 22.95 | 3.16 | 3.32 | 24.12 | 2.53 | 30.15 | 104.24 | 0.37 |
| L-type | 81.47 | 10.88 | 25.01 | 7.49 | 3.26 | 20.01 | 4.07 | 94.30 | 2.74 |
| Nodal Roots | 297.49 | 10.71 | 390.83 | 27.79 | 0.76 | 312.66 | 0.95 | 102.38 | 11.74 |
| total | 528.08 | 335.39 | 419.57 | 1.57 | 1.26 | 335.66 | 1.57 | 83.26 | 7.10 |

L-type lateral length x 2.0

| Root Type | P uptake (ug) | RL (m) | RWt (mg) | RE-L (ug/m) | RE-Wt (ug/mg) | Cost (µg P) | Benefit/ cost | Benefit/cost vs Base | Cost Recovery |
|---|---|---|---|---|---|---|---|---|---|
| Root Hair | 160.91 | 606.09 | 1.19 | 0.27 | 135.16 | 0.95 | 168.95 | 95.56 | 0.06 |
| S-type | 171.01 | 55.36 | 7.62 | 3.09 | 22.44 | 6.10 | 28.05 | 96.99 | 0.37 |
| L-type | 365.84 | 43.96 | 100.79 | 8.32 | 3.63 | 80.63 | 4.54 | 105.08 | 2.30 |
| Nodal Roots | 299.66 | 10.78 | 396.47 | 27.80 | 0.76 | 317.18 | 0.94 | 101.66 | 11.06 |
| total | 997.43 | 716.19 | 506.07 | 1.39 | 1.97 | 404.86 | 2.46 | 130.38 | 4.24 |

Fast nodal root diameter (from 0.65-0.5 cm)

| Root Type | P uptake (ug) | RL (m) | RWt (mg) | RE-L (ug/m) | RE-Wt (ug/mg) | Cost (µg P) | Benefit/ cost | Benefit/cost vs Base | Cost Recovery |
|---|---|---|---|---|---|---|---|---|---|
| Root Hair | 90.44 | 395.13 | 0.78 | 0.23 | 116.53 | 0.62 | 145.66 | 82.39 | 0.07 |
| S-type | 107.92 | 33.79 | 4.73 | 3.19 | 22.81 | 3.78 | 28.52 | 98.58 | 0.38 |
| L-type | 171.26 | 21.70 | 49.30 | 7.89 | 3.47 | 39.44 | 4.34 | 100.56 | 2.46 |
| Nodal Roots | 262.73 | 10.73 | 286.20 | 24.48 | 0.92 | 228.96 | 1.15 | 123.48 | 9.33 |
| total | 632.36 | 461.35 | 341.01 | 1.37 | 1.85 | 272.81 | 2.32 | 122.67 | 4.62 |

**References**


Adem, G.D., Ueda Y., Hayes P.E., Wissuwa, M., (2020). Genetic and physiological traits for internal phosphorus utilization efficiency in rice. (2020) PLOS ONE
https://doi.org/10.1371/journal.pone.0241842

Brown, L. K., George, T. S., Thompson, J. A., Wright, G., Lyon, J., Dupuy, L., et al. (2012). What are the implications of variation in root hair length on tolerance to phosphorus deficiency in combination with water stress in barley (*Hordeum vulgare*)? Ann. Bot. 110:2, 319–328.
doi: 10.1093/aob/mcs085

De Bauw, P., Mai, T. H., Schnepf, A., Merckx, R., Smolders, E., and Vanderborght, J. (2020). A functional-structural model of upland rice root systems reveals the importance of laterals and growing root tips for phosphate uptake from wet and dry soils. Ann. Bot. 126:4, 789–806.
doi: /10.1093/aob/mcaa120

Diagne, A., Amovin-Assagba, E., Koichi, F., and Wopereis, M.C.S. (2013). "Estimation of cultivated area, number of farming households and yield for major rice-growing environments in Africa", in Realizing Africa's rice promise, ed. M.C.S. Wopereis, D.E. Johnson, N. Ahmadi, E. Tollens, A. Jalloh (Boston, MA: CABI), 35–45

Dramé, N.K., and Manneh, B. (2013) "Rice Genetic Improvement for Abiotic Stress Tolerance in Africa", in Realizing Africa's rice promise, ed. M.C.S. Wopereis, D.E. Johnson, N. Ahmadi, E. Tollens, A. Jalloh (Boston, MA: CABI), 144–160
Fageria, N.K., Moreira, A., dos Santos, A.B. (2013). Phosphorus uptake and use efficiency in field crops. J. Plant Nutr. 36:13 2013-2022
doi: 10.1080/01904167.2013.816728.

Freschet, G.T., Roumet, C., Comas, L.H., Weemstra, M., Bengough, A.G., Rewald, B. et al. (2020), Root traits as drivers of plant and ecosystem functioning: current understanding, pitfalls and future research needs. New Phytol. Accepted Author Manuscript.
doi: 10.1111/nph.17072

Gahoonia, T. S., and Nielsen, N. E. (1998). Direct evidence on participation of root hairs in phosphorus (32P) uptake from soil. Plant Soil 198, 147–152.
doi: 10.1023/A:1004346412006
Ho M.D., Rosas J.C., Brown K.M., Lynch J.P. (2005). Root architectural tradeoffs for water and phosphorus acquisition. Functional Plant Biology 32, 737-748.

IRRI World Rice Statistics, (2020) Rice Yields in Asia. http://ricestat.irri.org:8080/wrsv3/entrypoint.htm [Accessed July 26, 2019]

Kirk, G.L.D., Santos, E.E., and Findenegg, G.R. (1999). Phosphate solubilization by organic anion excretion from rice (Oryza sativa L.) growing in aerobic soil. Plant Soil 211: 11-18

Mori, A., Fukuda, T., Vejchasarn, P., Nestler, J., Pariasca-Tanaka, J., and Wissuwa, M. (2016). The role of root size versus root efficiency in phosphorus acquisition in rice. J Exp. Bot. 67:4 1179-89.
doi: 10.1093/jxb/erv557

Morita, S. and Abe, J. (1994) "Modeling Root System Morphology in Rice" in Biology of Adventitious Root Formation, ed. T.D. Davis, B.E. Haissig (Boston, MA: SSBM)
doi: 10.1007/978-1-4757-9492-2_15

Murphy J., Riley J.P., A modified single solution method for the determination of phosphate in natural waters (1962), Anal. Chim. Acta. 27, 31-36.
doi: 10.1016/S0003-2670(00)88444-5.

Nestler, J., and Wissuwa, M. (2016). Superior Root Hair Formation Confers Root Efficiency in Some, But Not All, Rice Genotypes upon P Deficiency. Front. Plant Sci., 7, 1935.
doi: 10.3389/fpls.2016.01935

Nestler, J., Keyes, S. D., and Wissuwa, M. (2016). Root hair formation in rice (Oryza sativa L.) differs between root types and is altered in artificial growth conditions. J. Exp. Bot. 67, 3699–3708.
doi: 10.1093/jxb/erw115

Nigatu, G., Hansen, J., Childs, N., and Seeley, R. (2017). Sub-Saharan Africa is Projected To Be the Leader in Global Rice Imports" Amber Waves 9.
doi: 10.22004/AG.ECON.266026

Postma, J. A., Kuppe, C., Owen, M. R., Mellor, N., Griffiths, M., Bennett, M. J., et al. (2017). OpenSimRoot: widening the scope and application of root architectural models. New Phytol. 215:3, 1274-1286.
doi: /10.1111/nph.14641

Rebouillat, J., Dievart, A., Verdeil, J.L., et al. (2009). Molecular Genetics of Rice Root Development. Rice 2, 15–34.
doi: /10.1007/s12284-008-9016-5

Rose, T. J., Impa, S. M., Rose, M. T., Pariasca-Tanaka, J., Mori, A., Heuer, S., et al. (2012). Enhancing phosphorus and zinc acquisition efficiency in rice: a critical review of root traits and their potential utility in rice breeding. Ann. Bot. 112, 331–345.
doi: 10.1093/aob/mcs217

Saito, K., Vandamme, E., Johnson, J.M., Tanaka, A., Senthilkumar, K., Dieng, I, et al. (2019). Yield-limiting macronutrients for rice in sub-Saharan Africa. Geoderma. 338, 546-554
doi: 10.1016/j.geoderma.2018.11.036.

Silberbush M., and Barber S. (1983). Phosphorus and Potassium Uptake of Field-Grown Soybean Cultivars Predicted by a Simulation Model. Soil Sci. Soc. Am. J. 48:3, 592-596.

Silberbush M., and Barber S. (1983). Sensitivity of simulated phosphorus uptake to parameters used by a mechanistic-mathematical model. Plant Soil 74:1 93-100.

Tsujimoto, Y., Rakotoson, T., Tanaka, A., and Saito, K. (2019). Challenges and opportunities for improving N use efficiency for rice production in sub-Saharan Africa. Plant Prod. Sci. 22:4, 413-427.
doi: 10.1080/1343943X.2019.1617638.

Vandamme, E., Rose, T., Saito, K., Jeong, K., and Wissuwa, M. (2015). Integration of P acquisition efficiency, P utilization efficiency and low grain P concentrations into P-efficient rice genotypes for specific target environments. Nutr. Cycl. Agroecosyst. 104, 413–427.
doi: 10.1007/s10705-015-9716-3

Wissuwa, M., and Ae, N. (2001). Genotypic variation for tolerance to phosphorus deficiency in rice and the potential for its exploitation in rice improvement. Plant Breed. 120, 43–48.
doi: 10.1046/j.1439-0523.2001.00561.x

Wissuwa, M., Kondo, K., Fukuda, T., Mori, A., Rose, M.T., Pariasca‐Tanaka, J et al. (2015)
Unmasking novel loci for internal phosphorus utilization efficiency in rice germplasm through Genome‐Wide Association Analysis. PLoS One, 10:4, e0124215..

Wissuwa, M., Gonzalez, D., and Watts-Williams, S.J. (2020). The contribution of plant traits and soil microbes to phosphorus uptake from low-phosphorus soil in upland rice varieties. Plant Soil 448, 523–537.
doi: /10.1007/s11104-020-04453-z

Zygalakis, K. C., Kirk, G. J. D., Jones, D. L., Wissuwa, M., and Roose, T. (2011). A dual porosity model for nutrient uptake by root hairs. *New Phytol.* 192, 676–688. doi: 10.1111/j.1469-8137.2011.03840.x